Hindawi
Journal of Energy
Volume 2018, Article ID 6968023, 10 pages
https://doi.org/10.1155/2018/6968023

Research Article

Behavior of a Dual Stator Induction Machine Fed by Neutral Point Clamped Multilevel Inverter

Mohamed Arbi Khlifi [1,2]

[1] *Department of Electrical Engineering, University of Hail, Hail, Saudi Arabia*
[2] *Research Laboratory SIME, University of Tunis, National School of Engineers of Tunis (ENSIT), Tunis, Tunisia*

Correspondence should be addressed to Mohamed Arbi Khlifi; medarbi.khlifi@gmail.com

Received 19 March 2018; Revised 29 August 2018; Accepted 23 September 2018; Published 10 October 2018

Academic Editor: Ciro Aprea

Use of multilevel inverters with induction machines has become popular in most energy conversion and management systems. The present paper discusses the behavior of the dual stator-winding induction machine (DSIM) for the power source, which is a power supply with Neutral Point Clamped (NPC). Multilevel inverter with PWM technique control is analyzed. The DSIM control is obtained by the PWM technique to multicarrier PWM technique and after a comparative study of various characteristics of the DSIM taking into account the different electrical offsets between the two stars (0°, 30°, 60°). The gap between the two stars was considered, and it is impacted on torque and rates harmonic distortion of circulation currents.

1. Introduction

Induction machines with n-phase symmetrical have an equal angle between the successive phases of the stator a=2p/n. It is assumed that the windings are distributed sinusoidal, so that all higher spatial harmonics of the magnetomotive force can be neglected. The machines with odd number of phase have the distinction of eliminating the first harmonic of the larger current, harmonic "5" with pentaphase machine, and the harmonic "7" with heptaphase machine [1–4].

One of the main objectives of the multiphase machines and the reliability are known; for example, in the case of multistar machinery for failure in a phase we just need to disconnect the star that contains the faulty phase, which reduces torque, deployed 50% with a significant increase in torque ripples and magnetic Song [5–8]. Through the history of multiphase machines, the most popular multiphase machine type has been a dual three-phase machine. Dual three-phase machines are characterized by the multiphase structure with two sets of three-phase stator windings in the same stator frame. As a disadvantage, dual three-phase machines can suffer from problems with undesired stator current harmonics [9–11].

When power is increased, problems arise both in the voltage inverter and in the machine itself. The static switches of the voltage inverter must switch high currents and it is often necessary to place several structures in parallel, given power, reducing switching currents through the voltage increase. The inverter voltage PWM technique imposes high voltage gradients, thus causing accelerated aging of insulating [4, 12–14].

To avoid this, one among the possible solutions is the large number of phases leading to distribute the power supplied to the machine. Another solution is to conduct multilevel inverters providing a supply of better quality while requiring smaller sizes switches (IGBT). This allows for simple structures and tested for inverters, with reduced thermal problems and electromagnetic interference [3, 15, 16].

The idea of a machine with several windings is born in order to have two separate windings. Compared with the conventional machine, having a second winding facilitates control of the speed of the machine and transmits significant power through a static converter.

Multiphase machines are machines whose number of phases q is greater than three and can provide more compared to three-phase machines because they cannot obey the

requirements requested in specific application areas; they are developed mainly in the field of training for variable speed high power because the multiplication of the number of phases allows on the one hand improving the safety of the operation until at least three phases are active; there may be up to three phases open without the neutral connection which is required on the other hand to reduce the size of components in power modulators of energy.

These constraints make the multiphase machine a very interesting concept; it is present in the fields of marine, rail traction, the petrochemical industry, avionics, automotive, etc. [17–20].

The best known multiphase machine is probably the dual stator-winding induction machine whose two stars are identical and share the same stator and are phase shifted by an angle of 30°. Its windings have the same number of poles and are supplied at the same frequency. The structure of the rotor is identical to that of a three-phase machine, so it can be either squirrel cage or wound to form a three-phase winding.

2. Mathematical Model of Dual Stator Induction Motor

A dual three-phase machine is the most common multiphase machine structure. Dual three-phase machines have two sets of three-phase stator windings in the same stator frame. Displacement between the winding sets can take different values. However, only 0, 30, or 60 electrical degrees are actually encountered in practice. If the winding sets are not spatially shifted, the resulting machine is essentially a conventional three-phase machine with two parallel winding sets. On the other hand, displacing the winding set by 60 electrical degrees results in a symmetrical six-phase machine. Although both of these alternatives can offer some advantages, the most popular solution is that the star which connected three-phase stator windings is spatially shifted by 30 electrical degrees, and the neutral points of the sets are galvanic ally isolated from each other.

(i) The phases of the first star are sa_1, sb_1, and sc_1, phases which take the second star are sa_2, sb_2, and sc_2, and rotor phases are marked by ra, rb, and rc.

(ii) α expresses the angle of displacement between the two stars.

(iii) θ_1 expresses the position of the rotor (phase ra) compared to a star (phase sa_1).

(iv) θ_2 expresses the position of the rotor (phase ra) compared to a star (phase sa_2).

(v) The operation of the machine is assumed without saturation of magnetic circuit and neglecting the effect of hysteresis and Foucault currents.

(vi) The construction of the machine is assumed to be homogeneous.

(vii) The magnetomotive force created by each phase of the two frames is sinusoidal distribution.

(viii) The two-phase stator windings are balanced and identical.

Taking into account the simplifying assumptions mentioned above and notation of vectors of quantities of voltage, current, and flux, we can write the following vectors:

For star 1,

$$\begin{aligned}[V_{s1}] &= [V_{as1} \quad V_{bs1} \quad V_{cs1}]^T \\ [I_{s1}] &= [I_{as1} \quad I_{bs1} \quad I_{cs1}]^T \\ [\phi_{s1}] &= [\phi_{as1} \quad \phi_{bs1} \quad \phi_{cs1}]^T\end{aligned} \tag{1}$$

For star 2,

$$\begin{aligned}[V_{s2}] &= [V_{as2} \quad V_{bs2} \quad V_{cs2}]^T \\ [I_{s2}] &= [I_{as2} \quad I_{bs2} \quad I_{cs2}]^T \\ [\phi_{s2}] &= [\phi_{as2} \quad \phi_{bs2} \quad \phi_{cs2}]^T\end{aligned} \tag{2}$$

For rotor,

$$\begin{aligned}[V_r] &= [V_{ar} \quad V_{br} \quad V_{cr}]^T \\ [I_r] &= [I_{ar} \quad I_{br} \quad I_{cr}]^T \\ [\phi_r] &= [\phi_{ar} \quad \phi_{br} \quad \phi_{cr}]^T\end{aligned} \tag{3}$$

The electric equations of star 1 and star 2 and of rotor are, respectively, expressed by

$$[V_{s1}] = [R_{s1}] \cdot [I_{s1}] + \frac{d}{dt}[\phi_{s1}] \tag{4}$$

$$[V_{s2}] = [R_{s2}] \cdot [I_{s2}] + \frac{d}{dt}[\phi_{s2}] \tag{5}$$

$$[V_r] = [R_r] \cdot [I_r] + \frac{d}{dt}[\phi_r] \tag{6}$$

Expressions flux is as follows:

$$[\phi_{s1}] = [L_{s1,s1}][I_{s1}] + [M_{s1,s2}][I_{s2}] + [M_{s1,r}][I_r] \tag{7}$$

$$[\phi_{s2}] = [M_{s2,s1}][I_{s1}] + [L_{s2,s2}][I_{s2}] + [M_{s2,r}][I_r] \tag{8}$$

$$[\phi_r] = [M_{r,s1}][I_{s1}] + [M_{r,s2}][I_{s2}] + [L_{r,r}][I_r] \tag{9}$$

where $[R_{s1}]$, $[R_{s2}]$, $[R_r]$ are the stator resistance matrix (star 1 and 2) and rotor andL_{s1}, L_{s2}, L_r are the leakages inductances of one phase of star 1, star 2, and the rotor.

$$\begin{aligned}[M_{s2,s1}] = [M_{s1,s2}]^T = [M_{r,s1}] = [M_{s1,r}]^T = [M_{r,s2}] \\ = [M_{s2,r}]^T\end{aligned} \tag{10}$$

During the application of the d-q transformation and making the necessary manipulations, (4), (5), and (6) in d-q become

$$V_{ds1} = R_{s1}.i_{ds1} + \frac{d\phi_{ds1}}{dt} - w_a\phi_{qs1} \tag{11}$$

$$V_{qs1} = R_{s1}.i_{qs1} + \frac{d\phi_{qs1}}{dt} + w_a\phi_{ds1} \tag{12}$$

$$V_{ds2} = R_{s2}.i_{ds2} + \frac{d\phi_{ds2}}{dt} - w_a\phi_{qs2} \tag{13}$$

$$V_{qs2} = R_{s2}.i_{qs2} + \frac{d\phi_{qs2}}{dt} + w_a\phi_{ds2} \tag{14}$$

$$0 = R_r.i_{dr} + \frac{d\phi_{dr}}{dt} - (w_a - w)\,\phi_{q_r} \tag{15}$$

$$0 = R_r.i_{qr} + \frac{d\phi_{qr}}{dt} + (w_a - w)\,\phi_{dr} \tag{16}$$

with $w = d(\psi - \theta_m)/dt$ being speed of rotation of the coordinate (d, q) relative to the rotor and$w_a = d\psi/dt$ being speed of rotation of the coordinate (d, q) relative to star 1.
Applying the Park transformation on the equations of flux, we obtain

$$\begin{aligned}
\phi_{ds1} &= L_{s1}i_{ds1} + \frac{3}{2}L_{ms}i_{ds1} + \frac{3}{2}L_{ms}i_{ds2} + \frac{3}{2}M_{sr}i_{dr}\\
\phi_{qs1} &= L_{s1}i_{qs1} + \frac{3}{2}L_{ms}i_{qs1} + \frac{3}{2}L_{ms}i_{qs2} + \frac{3}{2}M_{sr}i_{qr}\\
\phi_{ds2} &= L_{s2}i_{ds2} + \frac{3}{2}L_{ms}i_{ds2} + \frac{3}{2}L_{ms}i_{ds1} + \frac{3}{2}M_{sr}i_{dr}\\
\phi_{qs2} &= L_{s2}i_{qs2} + \frac{3}{2}L_{ms}i_{qs2} + \frac{3}{2}L_{ms}i_{qs1} + \frac{3}{2}M_{sr}i_{qr}\\
\phi_{dr} &= L_r i_{dr} + \frac{3}{2}L_{mr}i_{dr} + \frac{3}{2}M_{sr}i_{ds1} + \frac{3}{2}M_{sr}i_{ds2}\\
\phi_{qr} &= L_r i_{qr} + \frac{3}{2}L_{mr}i_{qr} + \frac{3}{2}M_{sr}i_{qs1} + \frac{3}{2}M_{sr}i_{qs2}
\end{aligned} \tag{17}$$

$$\frac{3}{2}L_{ms} = \frac{3}{2}L_{mr} = \frac{3}{2}M_{sr} = L_m \tag{18}$$

with L_m being the cyclic mutual inductance between star 1, star 2, and the rotor.
The previous system of equations becomes

$$\phi_{ds1} = L_{s1}.i_{ds1} + L_m\left(i_{ds1} + i_{ds2} + i_{dr}\right) \tag{19}$$

$$\phi_{qs1} = L_{s1}.i_{qs1} + L_m\left(i_{qs1} + i_{qs2} + i_{qr}\right) \tag{20}$$

$$\phi_{ds2} = L_{s2}.i_{ds2} + L_m\left(i_{ds1} + i_{ds2} + i_{dr}\right) \tag{21}$$

$$\phi_{qs2} = L_{s2}.i_{qs2} + L_m\left(i_{qs1} + i_{qs2} + i_{qr}\right) \tag{22}$$

$$\phi_{dr} = L_r.i_{dr} + L_m\left(i_{ds1} + i_{ds2} + i_{dr}\right) \tag{23}$$

$$\phi_{qr} = L_r.i_{qr} + L_m\left(i_{qs1} + i_{qs2} + i_{qr}\right) \tag{24}$$

with $L_{s1}+L_m$ being the cyclic inductance of the star 1; $L_{s2}+L_m$ being the cyclic inductance of the star 2; $L_r + L_m$ being the cyclic inductance of the rotor.
The electromagnetic torque can be expressed by

$$C_{em} = p\left(\phi_{ds1}i_{qs1} - \phi_{qs1}i_{ds1} + \phi_{ds2}i_{qs2} - \phi_{qs2}i_{ds2}\right) \tag{25}$$

By introducing the equations of flux (19) and (20) in (25) we obtain

$$C_{em} = pL_m\left[\left(i_{qs1} + i_{qs2}\right)i_{dr} - \left(i_{ds1} + i_{ds2}\right)i_{qr)}\right] \tag{26}$$

Introducing the equations of current i_{dr} and i_{qr} in (25) we obtain

$$C_{em} = p\frac{L_m}{L_m + L_r}\left[\left(i_{qs1} + i_{qs2}\right)\phi_{dr} - \left(i_{ds1} + i_{ds2}\right)\phi_{qr}\right] \tag{27}$$

For a reference frame related to the stator ($w_a = 0$) we can obtain the state equation of the form

$$\dot{X} = AX + BU \tag{28}$$

with $X = [\phi_{ds1}\ \phi_{qs1}\ \phi_{ds2}\ \phi_{qs2}\ \phi_{dr}\ \phi_{qr}]$ being state vector and $U = [V_{ds1}\ V_{qs1}\ V_{ds2}\ V_{qs2}]$ being input vector.
After a calculation, we obtain the following matrices:

$$A = \begin{bmatrix}
\frac{L_a - L_{s1}}{T_{s1}L_{s1}} & 0 & \frac{L_a}{T_{s1}L_{s2}} & 0 & \frac{L_a}{T_{s1}L_r} & 0\\
0 & \frac{L_a - L_{s1}}{T_{s1}L_{s1}} & 0 & \frac{L_a}{T_{s2}L_{s1}} & 0 & \frac{L_a}{T_{s1}L_r}\\
\frac{L_a}{T_{s2}L_{s1}} & 0 & \frac{L_a - L_{s2}}{T_{s2}L_{s2}} & 0 & \frac{L_a}{T_{s2}L_r} & 0\\
0 & \frac{L_a}{T_{s2}L_{s1}} & 0 & \frac{L_a - L_{s2}}{T_{s2}L_{s2}} & 0 & \frac{L_a}{T_{s2}L_r}\\
\frac{L_a}{T_rL_{s1}} & 0 & \frac{L_a}{T_rL_{s2}} & 0 & \frac{L_a - L_r}{T_rL_r} & -w\\
0 & \frac{L_a}{T_rL_{s1}} & 0 & \frac{L_a}{T_rL_{s2}} & w & \frac{L_a - L_r}{T_rL_r}
\end{bmatrix} \tag{29}$$

$$B = \begin{bmatrix} 1 & 0 & 0 & 0 \\ 0 & 1 & 0 & 0 \\ 0 & 0 & 1 & 0 \\ 0 & 0 & 0 & 1 \\ 0 & 0 & 0 & 0 \\ 0 & 0 & 0 & 0 \end{bmatrix} \tag{30}$$

$$\text{With: } L_a = \frac{1}{(1/L_{s1}) + (1/L_{s2}) + (1/L_r) + (1/L_m)} \tag{31}$$

$$\begin{aligned} T_{s1} &= \frac{L_{s1}}{R_{s1}}; \\ T_{s2} &= \frac{L_{s2}}{R_{s2}}; \\ T_r &= \frac{L_r}{R_r} \end{aligned} \tag{32}$$

The dual stator-winding induction machine model, the NPC inverter model, and the controller were implemented in MATLAB. The reference reactive power of the outer stator was set to zero to ensure unity power factor of the grid.

3. Two Three-Level NPC VSI-DSIM Cascades

3.1. Two Three-Level NPC VSI Structures. The operating mode is to supply a DSIM by an inverter dual stator-winding, that is to say, six arms controlled by a PWM control, as shown in Figure 1.

In this case the first three arms (A, B, and C) supply the first star which are shifted 120° between them, the same for the other three arms (D, E, and F), but the two stars are shifted by an electrical angle α. Figure 1 shows the structural diagram of an inverter double star that supplies a double star load (standard R-L) [6].

The matrix below shows the simple voltages for the two stars with shifted angel (0°):

$$\begin{pmatrix} V_{AN_1}(t) \\ U_{BN_1}(t) \\ U_{CN_1}(t) \\ U_{DN_2}(t) \\ U_{EN_2}(t) \\ U_{FN_2}(t) \end{pmatrix} = \frac{1}{3} \cdot \begin{pmatrix} 2 & -1 & -1 & 0 & 0 & 0 \\ -1 & 2 & -1 & 0 & 0 & 0 \\ -1 & -1 & 2 & 0 & 0 & 0 \\ 0 & 0 & 0 & 2 & -1 & -1 \\ 0 & 0 & 0 & -1 & 2 & -1 \\ 0 & 0 & 0 & -1 & -1 & 2 \end{pmatrix} \begin{pmatrix} V_{AO}(t) \\ V_{BO}(t) \\ V_{CO}(t) \\ V_{DO}(t) \\ V_{EO}(t) \\ V_{FO}(t) \end{pmatrix}$$

$$= \frac{E}{3} \cdot \begin{pmatrix} 2 & -1 & -1 & 0 & 0 & 0 \\ -1 & 2 & -1 & 0 & 0 & 0 \\ -1 & -1 & 2 & 0 & 0 & 0 \\ 0 & 0 & 0 & 2 & -1 & -1 \\ 0 & 0 & 0 & -1 & 2 & -1 \\ 0 & 0 & 0 & -1 & -1 & 2 \end{pmatrix} \begin{pmatrix} C(1,1) \\ C(2,1) \\ C(3,1) \\ C(4,1) \\ C(5,1) \\ C(6,1) \end{pmatrix} \tag{33}$$

Writing the following matrix represents the composed voltages for the two stars:

$$\begin{pmatrix} U_{AB}(t) \\ U_{BC}(t) \\ U_{CA}(t) \\ U_{DE}(t) \\ U_{EF}(t) \\ U_{FD}(t) \end{pmatrix} = \begin{pmatrix} 1 & -1 & 0 & 0 & 0 & 0 \\ 0 & 1 & -1 & 0 & 0 & 0 \\ -1 & 0 & 1 & 0 & 0 & 0 \\ 0 & 0 & 0 & 1 & -1 & 0 \\ 0 & 0 & 0 & 0 & 1 & -1 \\ 0 & 0 & 0 & -1 & 0 & 1 \end{pmatrix} \begin{pmatrix} V_{AO}(t) \\ V_{BO}(t) \\ V_{CO}(t) \\ V_{DO}(t) \\ V_{EO}(t) \\ V_{FO}(t) \end{pmatrix} \tag{34}$$

$$= E \begin{pmatrix} 1 & -1 & 0 & 0 & 0 & 0 \\ 0 & 1 & -1 & 0 & 0 & 0 \\ -1 & 0 & 1 & 0 & 0 & 0 \\ 0 & 0 & 0 & 1 & -1 & 0 \\ 0 & 0 & 0 & 0 & 1 & -1 \\ 0 & 0 & 0 & -1 & 0 & 1 \end{pmatrix} \begin{pmatrix} C(1,1) \\ C(2,1) \\ C(3,1) \\ C(4,1) \\ C(5,1) \\ C(6,1) \end{pmatrix}$$

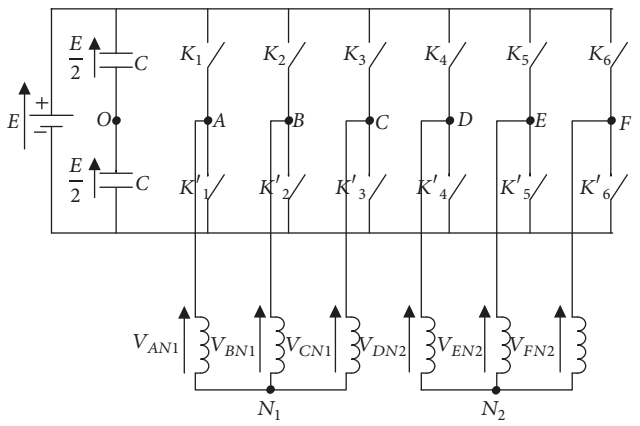

Figure 1: Structural diagram of an inverter double star.

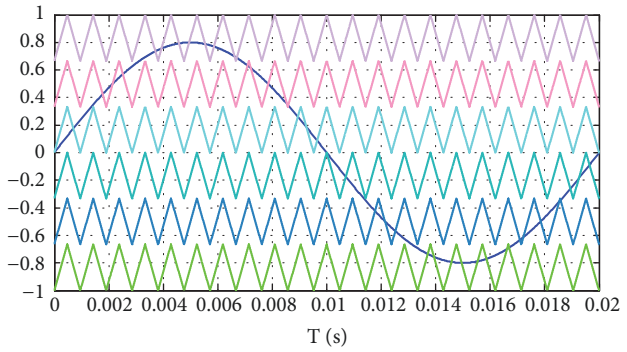

Figure 2: Principle of PWM technique (multicarrier PWM technique) for a seven-level inverter.

Voltages between the two nodes N_1 and N_2 are

$$V_{ON1}(t) = -\frac{1}{3}\left(\left(V_{AO}(t) + V_{BO}(t) + V_{CO}(t)\right)\right) \quad (35)$$

$$V_{ON2}(t) = -\frac{1}{3}\left(\left(V_{DO}(t) + V_{EO}(t) + V_{FO}(t)\right)\right) \quad (36)$$

$$V_{N_1N_2} = \frac{1}{3}\left(V_{AO} + V_{BO} + V_{CO} - V_{DO} - V_{EO} - V_{FO}\right) \quad (37)$$

These voltages are expressed in terms of control signals and the DC voltage where

$$V_{N_1N_2} = \frac{1}{3}E\left(2C(1,1) + 2C(2,1) + 2C(2,1) - 2C(4,1) - 2C(5,1) - 2C(6,1)\right) \quad (38)$$

3.2. PWM Strategy for the Two Three-Level NPC VSI. We adopted this technique (multicarrier PWM technique) to control the multilevel inverter. This technique is based on conventional sinusoidal modulation. It is the comparison of a sinusoidal signal called modulating wave over a triangular signal called carrier.

The PWM technique is to treat separately the case where the set point is positive and those where it is negative, as shown in Figure 2.

Table 1: relative torque ripple rate as function of the inverter levels number.

Levels number	Relative torque ripple rate in %
$m = 2$	45.2%
$m = 3$	10.52%
$m = 5$	5.1%
$m = 7$	4.96%

For an inverter with m levels, the command requires **(m-1)** triangular signals at the same frequency f_p and the same magnitude A_p (peak to peak).

The control signals of switches for the NPC inverter are obtained from the three reference sinusoidal signals phase shifted by $2\pi/3$, frequency f_m, and magnitude A_m.

PWM technique is characterized by two reports, the rate of modulation and the frequency ratio, defined as follows:

$$m_a = A_m/(m-1)A_p\text{: the rate of modulation.}$$

$$m_c = f_p/f_m\text{: the frequency ratio.}$$

3.3. Simulation of the DSIM Supplied by a Multilevel Inverter

3.3.1. Principle. To identify the simulation results, we will look at the evolution of electromagnetic, mechanical, electrical, and magnetic characteristics for the various levels of the inverter used, taking into account a shift $\alpha = 30^\circ$.

The simulation of the inverter at m levels has been established by the software "Matlab Simulink".

3.3.2. Results of Simulation. Figures 3–6 illustrate the evolution of the output voltage of an arm of the inverter when increasing the number of levels.

According to the results found there, when the level of the inverter voltage is m = 2 to m = 7, the output voltage approaches more and more perfect sinusoidal form.

Figures 7–10 illustrate the evolution of the electromagnetic torque and rotational speed for various levels of the inverter used.

Table 1 shows the rate of undulation on the following number of levels corresponding to.

The influence of the waveform of the supply voltage appears at the level of electromagnetic torque in steady state and has no influence on the shape of the characteristic speed of rotation.

4. Comparative Study of Various Characteristics of the DSIM Taking into Account the Different Electrical Offsets between the Two Stars (0°, 30°, 60°)

Figures 11, 12, and 13, respectively, represent the characteristic electromagnetic torque, rotational speed, and torque-speed characteristic of the DSIM supplied by a multilevel inverter (by 7 levels) for $\alpha = 0^\circ, 30^\circ, 60^\circ$ (see Tables 2 and 3).

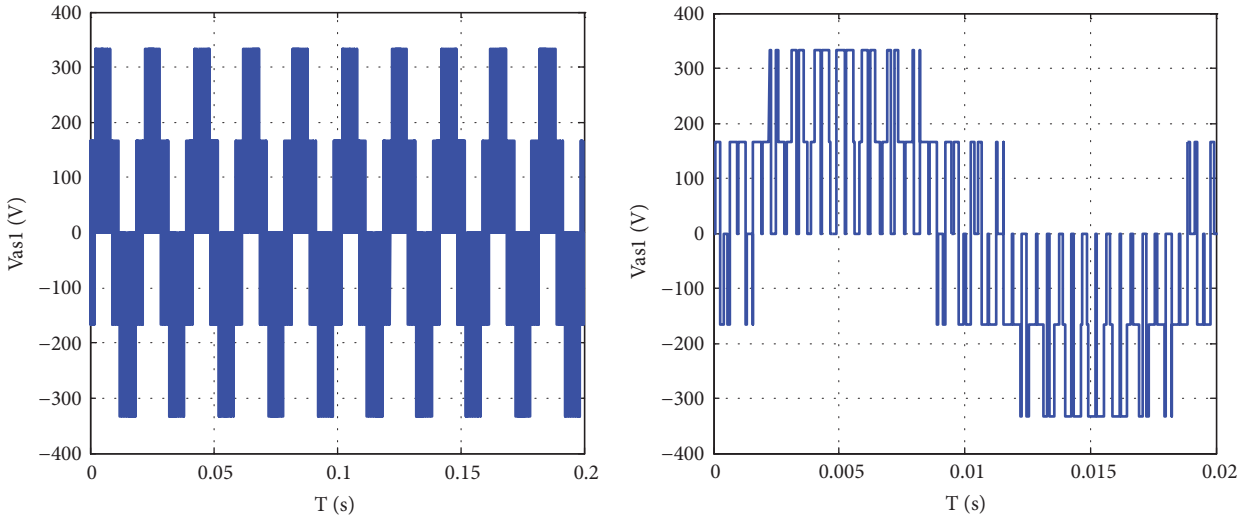

Figure 3: Waveform of output voltage V_{as1} for m=2.

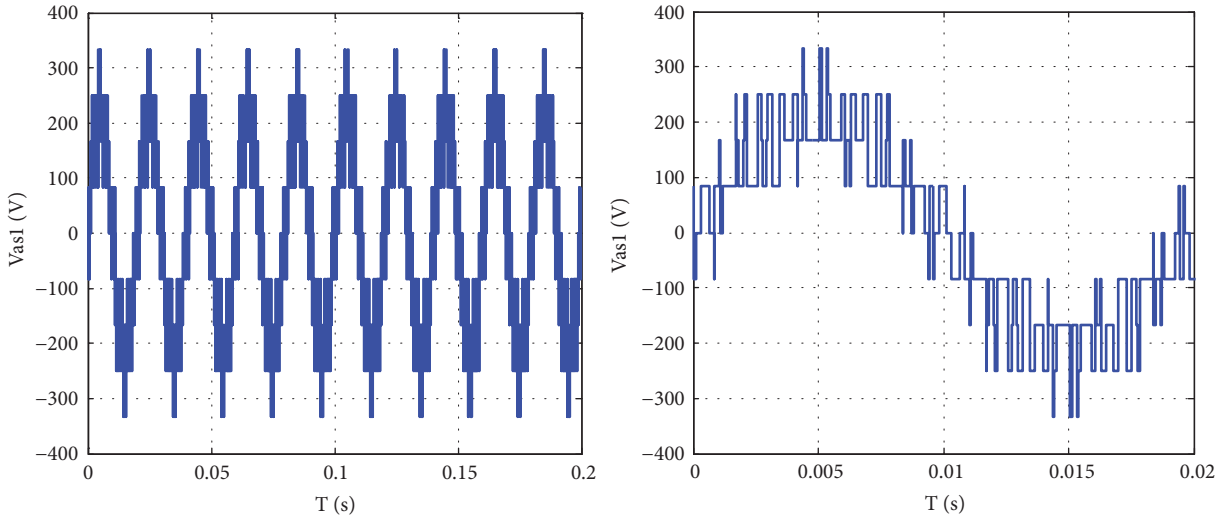

Figure 4: Waveform of output voltage V_{as1} for m=3.

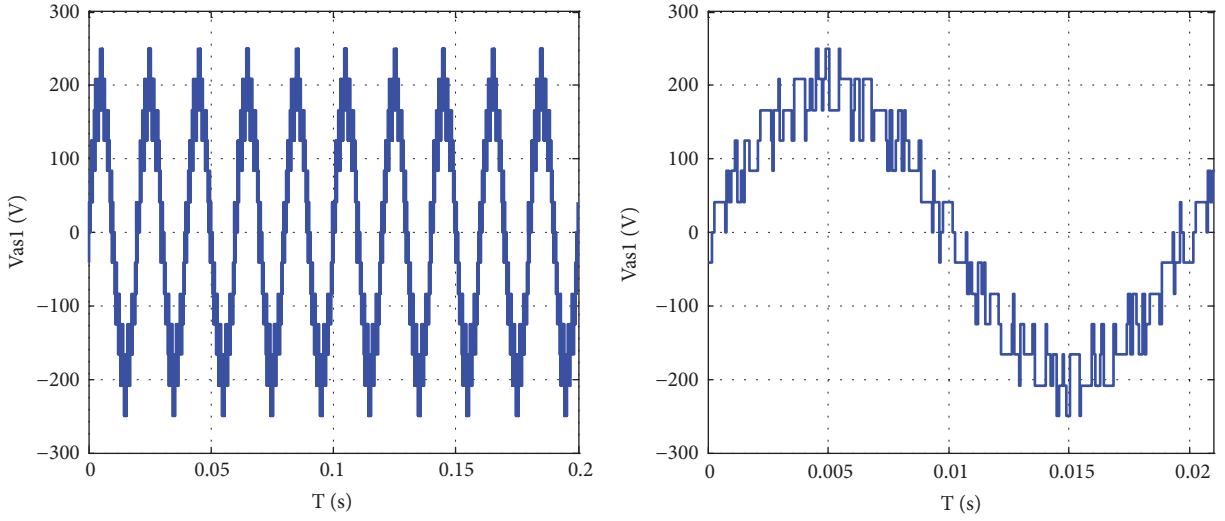

Figure 5: Waveform of output voltage V_{as1} for m=5.

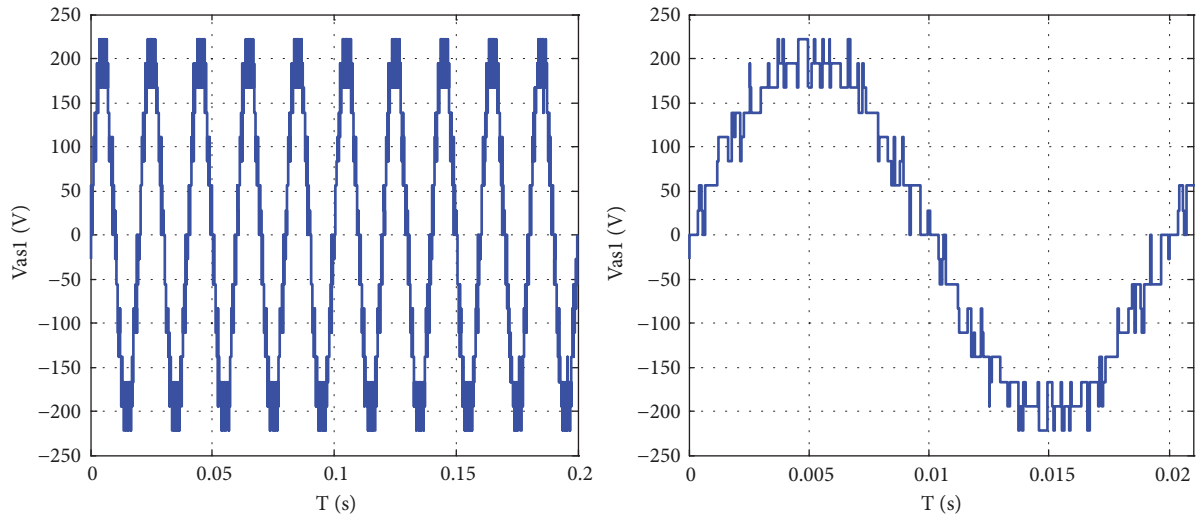

Figure 6: Waveform of output voltage V_{as1} for m=7.

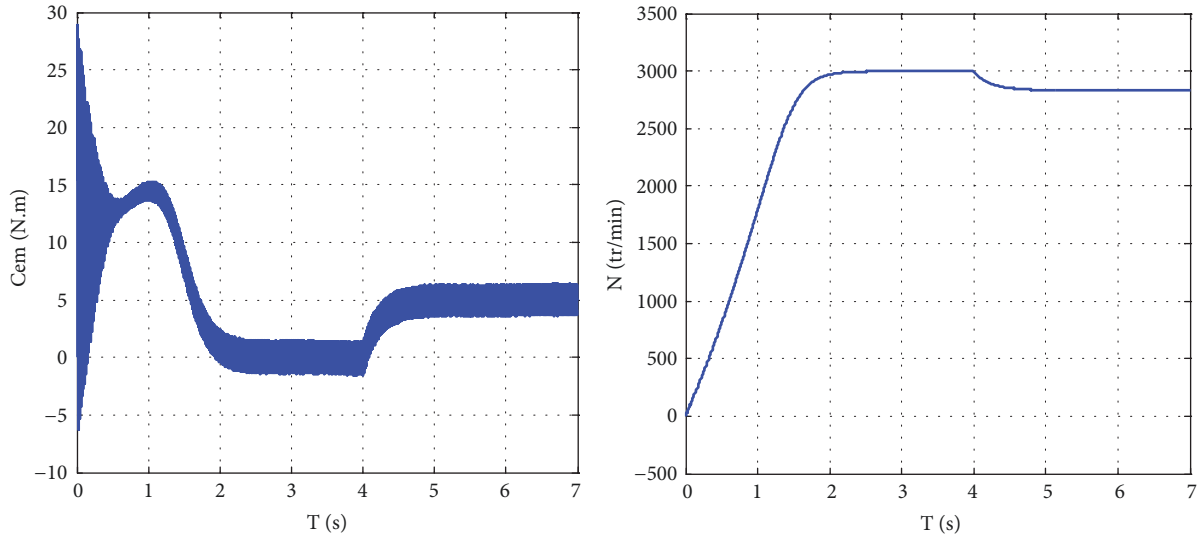

Figure 7: Electromagnetic torque and rotational speed for m = 2.

Table 2: relative torque ripple rate as function different shifts.

α	$\Delta C\%$
$\alpha = 0^{\circ}$	8.48%
$\alpha = 30^{\circ}$	4.96%
$\alpha = 60^{\circ}$	6.54%

Table 3: Effect of an angular offset on the operating characteristics of the DSIM.

	For α=0°	For α=30°	For α=60°
Peak torque	23.75 N.m	22.05 N.m	17.85 N.m
Average torque	12.37 N.m	11.36 N.m	9.22 N.m
settling time for torque	2.63 s	3.01 s	3.38 s
settling time for speed	2.49 s	3.02 s	3.43 s

5. Discussion

The simulation results found when combining inverter-DSIM are similar to results found by simulating the DSIM supplied by a balanced source direct, but with the presence of harmonics at the electromagnetic torque, the torque-speed characteristic, of the stator and rotor currents and flux.

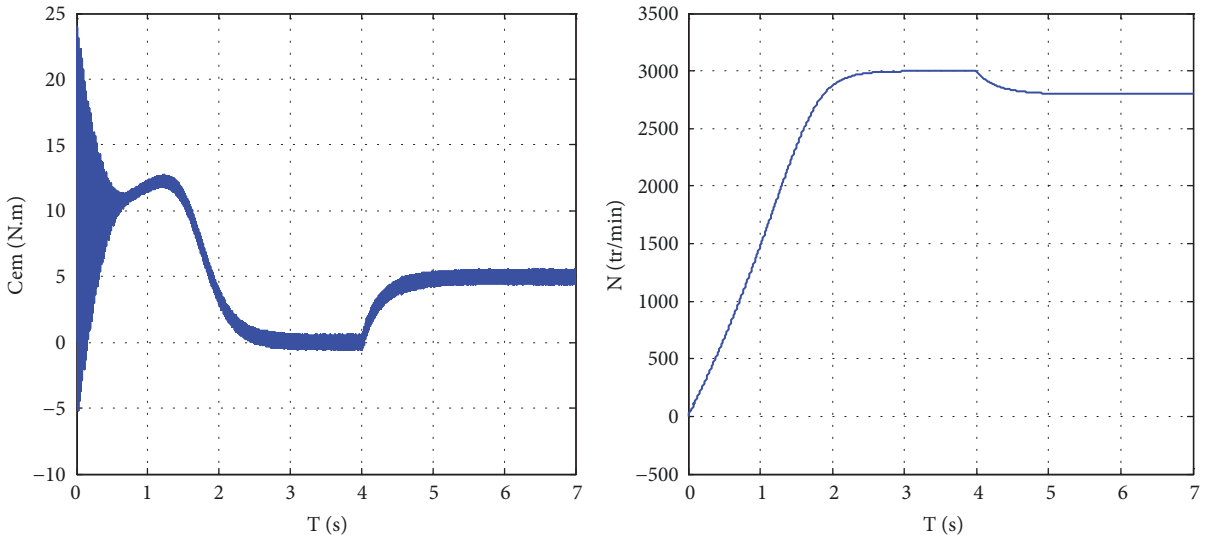

Figure 8: Electromagnetic torque and rotational speed for m = 3.

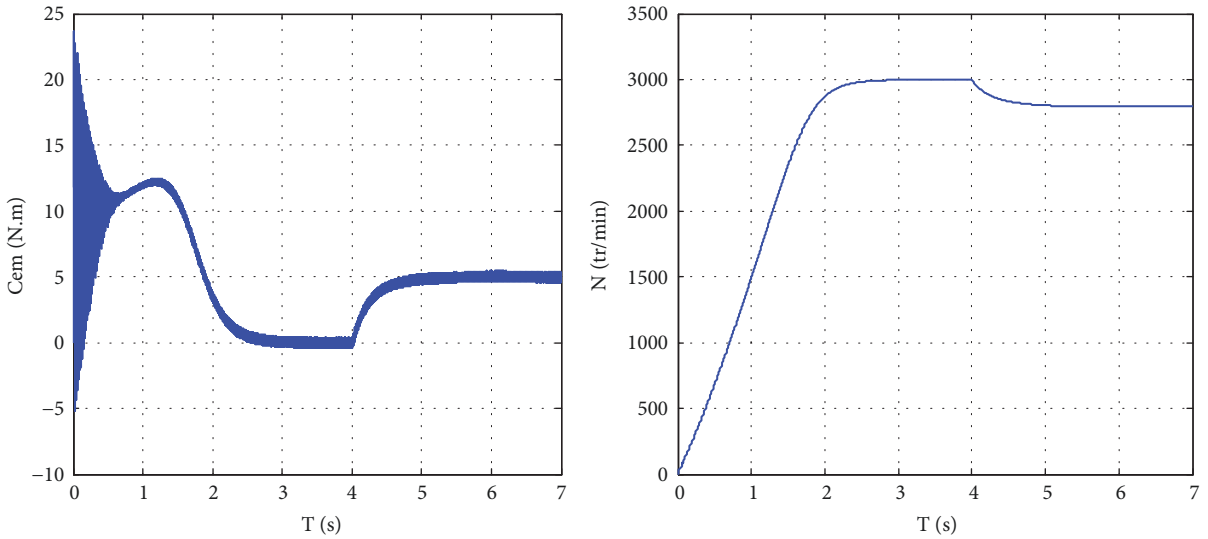

Figure 9: Electromagnetic torque and rotational speed for m = 5.

These harmonics are due to the presence of voltage inverters; they are decreasing gradually as the number of levels of the inverter increases.

In reality, static converters can provide a voltage (and current) cut (e), because the power electronics can be an electronic switching. To reduce the adverse effects of cutting the output voltage and thus tend slightly more to the "ideal converter", we shall increase the number of available output levels of the static converter. This will then reduce the amplitude of the voltage cut fronts, so the amplitude of the harmonic lines is induced by cutting.

6. Conclusion

This paper presents the impact of the multilevel NPC inverter sources on the circulating currents and voltage between the two stars of the DSIM. On the other hand, a higher level of output voltage of the multilevel inverter helps to improve a system of operation of the induction machine mainly by reducing the distortion of current consumption and electromagnetic torque ripple.

The minimization of voltage and current induces the decreasing of the THD and improving of the energy quality, which means the reduction of the torque ripples and the cleaning of the stator currents. The PWM give the better results. The results obtained by simulation (mechanical, electrical, and magnetic characteristics) confirm the validity of theoretical studies on the machine and established models.

Data Availability

The data used to support the findings of this study are available from the corresponding author upon request.

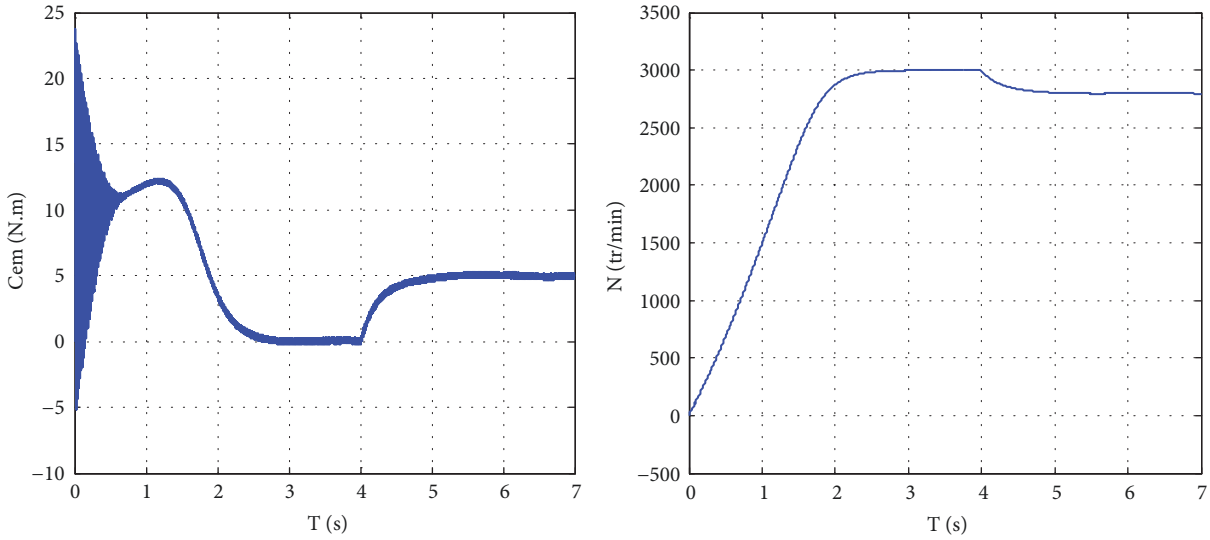

Figure 10: Electromagnetic torque and rotational speed for m = 7.

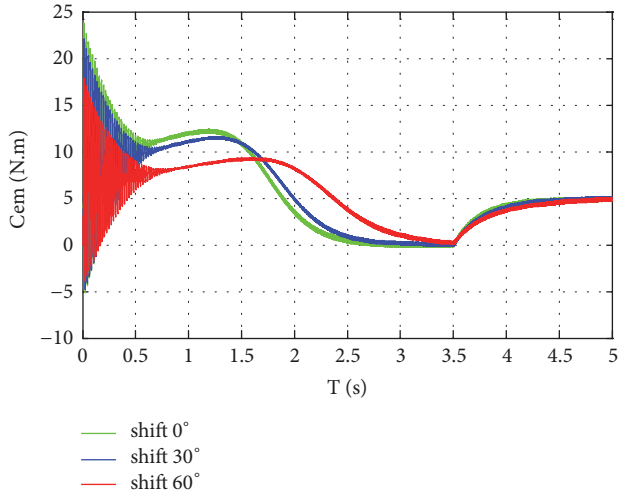

Figure 11: Characteristic electromagnetic torque.

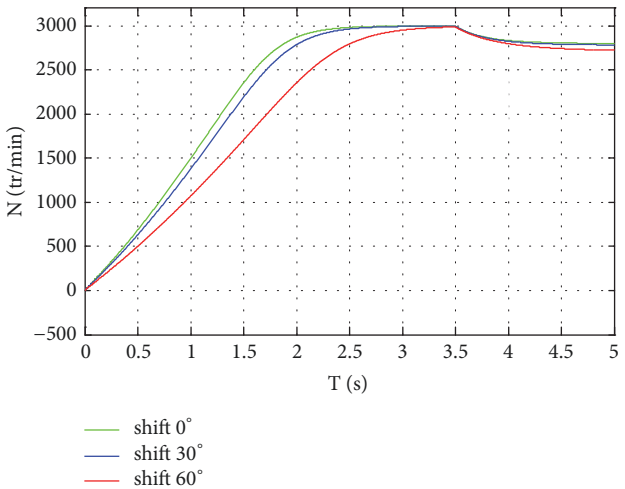

Figure 12: Characteristic of rotational speed.

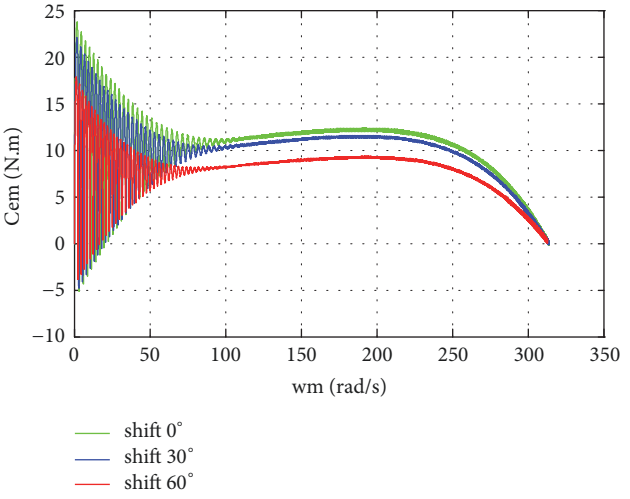

Figure 13: Torque-speed characteristic.

Conflicts of Interest

The author declares that they have no conflicts of interest.

References

[1] D. Chermiti, N. abid, and A. Khedher, "Voltage regulation approach to a self-excited induction generator: Theoretical study and experimental validation," *International Transactions on Electrical Energy Systems*, vol. 27, no. 5, 2017.

[2] A. Edpuganti and A. K. Rathore, "Optimal pulsewidth modulation for common-mode voltage elimination scheme of medium-voltage modular multilevel converter-fed open-end stator winding induction motor drives," *IEEE Transactions on Industrial Electronics*, vol. 64, no. 1, pp. 848–856, 2017.

[3] M. B. Slimene, M. A. Khlifi, and M. B. Fredj, "Sensorless speed control for dual stator induction motor drive using IFOC

strategy with magnetic saturation," *Applied Computational Electromagnetics Society Journal*, vol. 32, no. 3, pp. 262–267, 2017.

[4] M. Darijevic, M. Jones, O. Dordevic, and E. Levi, "Decoupled PWM Control of a Dual-Inverter Four-Level Five-Phase Drive," *IEEE Transactions on Power Electronics*, vol. 32, no. 5, pp. 3719–3730, 2017.

[5] Z. Wang, Y. Wang, J. Chen, and M. Cheng, "Fault-Tolerant Control of NPC Three-Level Inverters-Fed Double-Stator-Winding PMSM Drives Based on Vector Space Decomposition," *IEEE Transactions on Industrial Electronics*, vol. 64, no. 11, pp. 8446–8458, 2017.

[6] B. Mahato, R. Raushan, and K. C. Jana, "Modulation and control of multilevel inverter for an open-end winding induction motor with constant voltage levels and harmonics," *IET Power Electronics*, vol. 10, no. 1, pp. 71–79, 2017.

[7] J. Anitha Roseline, M. Senthil Kumaran, V. Rajini, and V. Subramaniyan, "Unified algorithm for multilevel inverters," *IET Power Electronics*, vol. 10, no. 7, pp. 808–816, 2017.

[8] B. S. Marwa, K. M. Larbi, B. F. Mouldi, and R. Habib, "Modeling and analysis of double stator induction machine supplied by a multi level inverter," in *Proceedings of the MELECON 2012 - 2012 16th IEEE Mediterranean Electrotechnical Conference*, pp. 269–272, Yasmine Hammamet, Tunisia, March 2012.

[9] D. Kouchih, N. Boumalha, M. Tadjine, and M. S. Boucherit, "New approach for the modeling of induction machines operating under unbalanced power system," *International Transactions on Electrical Energy Systems*, vol. 26, no. 9, pp. 1832–1846, 2016.

[10] G. Zhang, Z. Du, Y. Ni, and C. Li, "Nonlinear model reduction-based induction motor aggregation," *International Transactions on Electrical Energy Systems*, vol. 26, no. 2, pp. 398–411, 2016.

[11] H. Xu, F. Bu, W. Huang, Y. Hu, and H. Liu, "Control and Performance of Five-Phase Dual Stator-Winding Induction Generator DC Generating System," *IEEE Transactions on Industrial Electronics*, vol. 64, no. 7, pp. 5276–5285, 2017.

[12] Z. Wang, X. Wang, J. Cao, M. Cheng, and Y. Hu, "Direct Torque Control of T-NPC Inverters-Fed Double-Stator-Winding PMSM Drives with SVM," *IEEE Transactions on Power Electronics*, vol. 33, no. 2, pp. 1541–1553, 2018.

[13] Y. Park, J.-M. Yoo, and S.-K. Sul, "Vector Control of Double-Delta Sourced Winding for a Dual-Winding Induction Machine," *IEEE Transactions on Industry Applications*, vol. 53, no. 1, pp. 171–180, 2017.

[14] Z. Q. Zhu and B. Lee, "Integrated Field and Armature Current Control for Dual Three-Phase Variable Flux Reluctance Machine Drives," *IEEE Transactions on Energy Conversion*, vol. 32, no. 2, pp. 447–457, 2017.

[15] L. Han, X. Ou, J. Du, X. Han, and Y. Guo, "Study of Direct Coupling in Stator Dual Windings of a Brushless Doubly Fed Machine," *IEEE Transactions on Energy Conversion*, vol. 32, no. 3, pp. 974–982, 2017.

[16] Z. Nasiri-Gheidari and H. Lesani, "Theoretical modeling of axial flux squirrel cage induction motor considering both saturation and anisotropy," *International Transactions on Electrical Energy Systems*, vol. 24, no. 3, pp. 335–346, 2014.

[17] Z. Ali, S. K. Shahzad, and W. Shahzad, "Performance analysis of support vector machine based classifiers," *International Journal of ADVANCED AND APPLIED SCIENCES*, vol. 5, no. 9, pp. 33–38, 2018.

[18] R. Pahlavani, "Dynamic comparative advantage analysis of rural and pastoral systems of small ruminant husbandry," *International Journal of Advanced and Applied Sciences*, vol. 4, no. 11, pp. 81–87, 2017.

[19] Z. Abderrahim et al., "New modified direct torque control-fuzzy logic controller of doubly fed induction machine," *International Journal of Advanced and Applied Sciences*, vol. 4, no. 7, pp. 16–20, 2017.

[20] K. Y. Ahmed, "Development of power electronic distribution transformer using fuzzy logic control," *International Journal of Advanced And Applied Sciences*, vol. 5, no. 5, pp. 34–39, 2018.